5

Research of the Scattering of Non-linearly Interacting Plane Acoustic Waves by an Elongated Spheroid

Iftikhar B. Abbasov
Taganrog Technological Institute, Southern Federal University
Russia

1. Introduction

For the first time the problem of acoustic wave scattering on elongated spheroids was stated in works [Cpence & Ganger, 1951], [Burke, 1966], [Kleshchyov & Sheiba, 1970]. Work [Cpence & Ganger, 1951] considers the problem of sound scattering on a elongated spheroid with various boundary conditions. Work [Burke, 1966] considers the problem of sound scattering on a rigid spheroid in the long-wave approximation. Work [Kleshchyov & Sheiba, 1970] considers the problems of sound wave scattering on a elongated spheroid where angular characteristics for sound wave scattering on a soft and rigid elongated spheroid were found.

The studies of acoustic field of spheroidal radiators were considered in works [Chertock, 1961], [Andebura, 1969], where acoustic field, radiation impedance of arbitrary elongated spheroid were defined. Work [Andebura, 1976] considers integral characteristics of the interaction between spheroid and incident sound wave with different spheroid orientations relating to propagation direction of incident wave.

The diffraction problem of plane sound wave on elongated rigid revolution bodies within the field of small values of wave rate is considered in work [Fedoryuk, 1981], where scattering amplitude asymptotics are found. Work [Tetyuchin & Fedoryuk, 1989] describe plane sound wave diffraction on a elongated rigid revolution body in liquid, give calculation scattering diagrams on a steel and aluminium spheroid with lateral incidence of a plane wave.

Work [Boiko, 1983] considers the case of plane wave scattering on a thin revolution body that differs from medium with its contractiveness and density. The principal term of evanescent field asymptotics was found, angular characteristics for plane wave scattering by rigid elongated spheroid in geometrical scattering field were given.

The questions of sound scattering by gas-filled spheroidal fish-maw are considered in works [Haslett, 1962], [Babailov & Kanevskyi, 1988]. A fish-maw is given as a elongated soft spheroid, frequency-angle characteristics of inverse scattering are given as well as resonance characteristic spheroidal maw.

In recent decades a number of works devoted to sound scattering on spheroids were published by Kleshchyov A.A. [Kleshchyov, 1986; 1992; 2004]. These works are devoted to studies of sound scattering on fish and fish flock maws near surface and bottom. A gas maw

Source: Acoustic Waves, Book edited by: Don W. Dissanayake,
ISBN 978-953-307-111-4, pp. 466, September 2010, Sciyo, Croatia, downloaded from SCIYO.COM

is approximated by soft elongated spheroid; the flock is divided to a definite number of scatterers. The scattered sound is formed shape at the cost of signal interference, scattered by separate scatterers, on condition that the distance between scatterers is more than scatterer's dimensions. The fish flock is near one of the two boundarys: either water-air or water-bottom. At that it is assumed that the boundarys are plane and ideal, the air is replaced by vacuum, the bottom is ideally firm. Scattering characteristics of separate maws in the form of soft elongated spheroid are calculated with ranges from angular and radially spheroidal functions.

The problem of plane acoustic wave scattering on spheroidal shells was considered in works [Werby & Green, 1987], [Weksler et al., 1999]. These works study the surface waves directly on scatterers themselves, they describe frequency dependence of inverse scattering in farfield.

Some questions of experimental studies of acoustic wave scattering on elongated form bodies are considered in works [Stanton, 1989], [Lebedev & Salin, 1997].

Last years some works appeared, written by [Belkovich et al., 2002], [Kuzkin, 2003], devoted to acoustic wave scattering on spheroids in waveguides. This problem appears when active acoustic monitoring of Cetacea population in world's oceans and seas. The model problem of sound wave diffraction on elongated soft spheroids (Cetacea) is considered, when locating them in ocean waveguide. Diffuse sound field is analysed as a parameter function: spheroid dimensions, its position relative to sound source and detector, vertical profile of sound speed in waveguide, acoustic parameters of bottom boundary.

Except the works above devoted to linear scattering with spheroids, there are several works devoted to nonlinear acoustic spectroscopy [Guyer & Johnson, 1999], [Lebedev et al., 2005]. Work [Guyer & Johnson, 1999] considers the problem of nonlinear acoustic defect diagnosis in materials and formations. Work [Lebedev et al., 2005] is devoted to solving the problem of nonlinear defect acoustic spectroscopy in geomaterials. A cavity model in the form of oblate spheroid is taken as a defect. The crack on a thin bar is shown as an example of defect isolation problem solving.

However the problem of interacting acoustic wave scattering on elongated spheroid has not been under study before. It becomes one of current interest when using parametric acoustic array for remote diagnostics of aquatic medium. This problem can also appear within biological environment diagnostics, where high nonlinear nature and nonhomogeneities are in the near field of a radiating unit. This chapter studies the scattering problem of nonlinearly interacting plane acoustic waves on rigid elongated spheroid.

2. Wave problems in elongated spheroidal coordinates

When solving the problems of wave diffraction on elongated form bodies, confocal coordinates, spheroidal in particular, are often used. These coordinates are used within studying acoustic wave radiating and scattering by ellipsoids, cigar-shaped bodies, as well as within studying diffraction by circular apertures [Skudrzyk, 1971].

When studying diffraction on cigar-shaped bodies, the elongated spheroidal coordinates system is used. Coordinate surfaces are spheroids $\xi = const$ and two-sheeted hyperboloids $\eta = const$. The elongated spheroid is formed by ellipse rotation round its longer axis (Fig.1). Within ellipse rotation round shorter axis, the oblate spheroid is formed. A great number of revolution body surfaces can be described with the help of spheroidal coordinate systems. Orb and cylinder can be considered as special cases of spheroidal surfaces, a continued thin bar and disks are confluent spheroids.

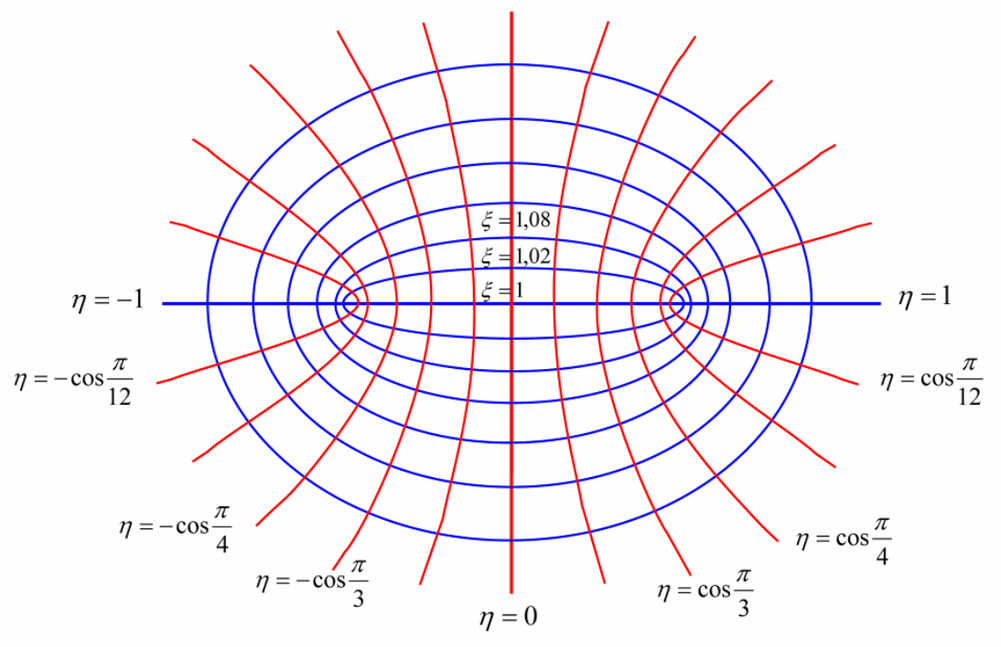

Fig. 1. Elliptic coordinate system

Ellipse is a geometrical locus, their sum of the distances r_1 and r_2 from two given points (focal points) is constant [Abramovitz & Stegun, 1971]:

$$r_1 + r_2 = const = \xi d\,, \qquad \text{or} \quad \frac{r_1 + r_2}{d} = \xi\,,$$

where d - distance between ellipse focuses, ξ - radial coordinate.
The length of ellipse longer axis L is (Fig.1) — $L = r_1 + r_2$, or $L = \xi d$, shorter axis D is defined from formula $D = d\sqrt{(\xi^2 - 1)}$.
Parameter ξ is an ellipse eccentricity measure - $e = d/L$, it follows that $\xi = 1/e$. With $\xi = 1$ ellipse degenerates into the interval with length d, with $\xi = \infty$ ellipse grades into circle of infinite radius. For long distances product ξd is equal in practice to duplicated distance from the origin of axis system.
The coordinate, equivalent to coordinate θ in a polar system, is obtained with the help of confocal hyperboloids (Fig.1)

$$\frac{r_1 - r_2}{d} = \eta = \cos\theta\,,$$

where η - angular coordinate.
The hyperbolic curve is a geometrical locus, their difference of the distances r_1 and r_2, from two given points (focal points F_1 and F_2) is constant (Fig.2). In spherical coordinates angle θ is an angle between radius-vector of observation point $M(\xi,\eta,\varphi)$ and coordinate axis x (Fig.3).
With larger coordinate value ξ spheroidal coordinates grade into spherical ones, and angle θ in formula $\eta = \cos\theta$ corresponds to asymptote angle for hyperbolic curve η.

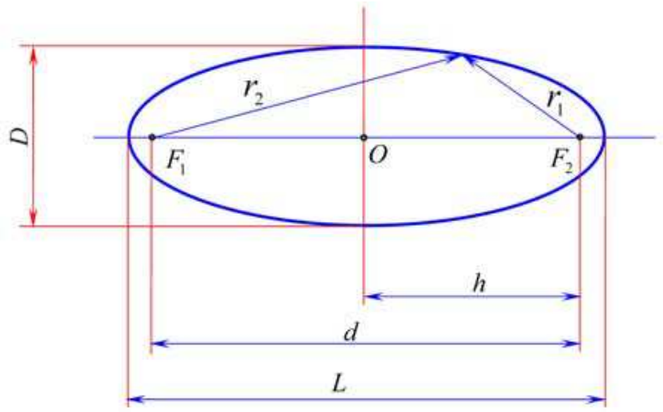

Fig. 2. Ellipse basic parameters

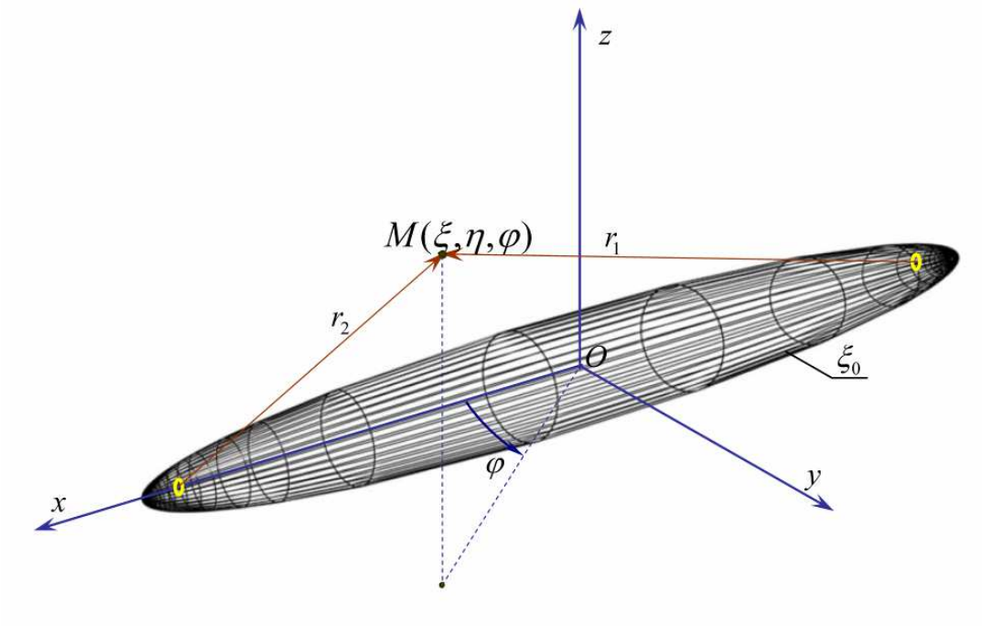

Fig. 3. Scatterer in elongated spheroidal coordinates system

3. Theory

To present the problem, the system of elongated spheroidal coordinates ξ, η, φ was chosen. The foci of the spheroid coincide with the foci of the spheroidal coordinate system. The spheroid is formed by the ellipse ξ_0 rotated about a major axis, which coincides with the x - axis of the Cartesian system. The geometry of the problem is presented in Fig.4. The coordinate surfaces are: for the spheroids - ξ=const and for the two-sheeted hyperboloids - η=const.

Elongated spheroidal coordinates are related to Cartesian coordinates by the following expressions [Tikhonov & Samarskyi, 1966]:

$$x = h_0 \xi \eta\,, \quad y = h_0 \sqrt{(\xi^2 - 1)(1 - \eta^2)}\cos\varphi\,, \quad z = h_0 \sqrt{(\xi^2 - 1)(1 - \eta^2)}\sin\varphi\,,$$

where $h_0 = d/2$, and d is the interfocal distance. Spheroidal coordinates ξ, η, φ are considered within the limits: $1 \le \xi < \infty$; $-1 \le \eta \le 1$; $0 \le \varphi \le 2\pi$.

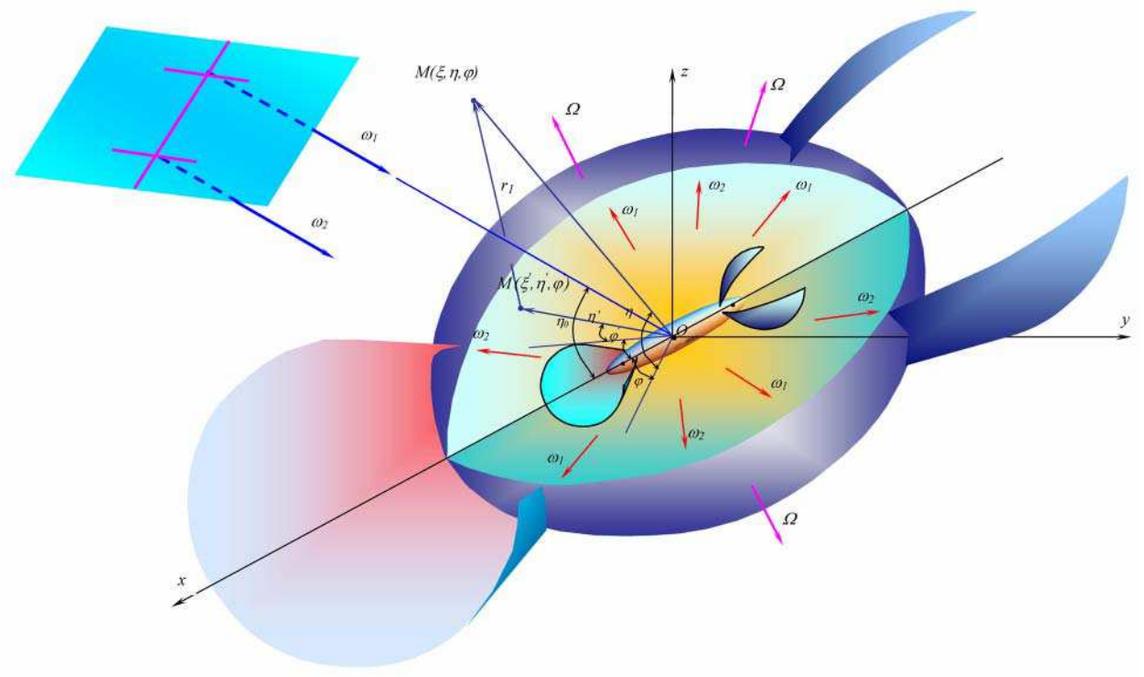

Fig. 4. Geometry of the problem

The perfect spheroid was put into homogeneous medium. The spheroid's surface is characterized by the coordinate ξ_0. Assuming that interacting plane high-frequency acoustic waves of the unit pressure amplitude falls on the spheroid at an arbitrary polar angle θ_0 (θ_0=arccosη_0) and an azimuthal angle φ_0, we express the acoustic pressure as:

$$p_{ni} = \exp\left[-i(k_n r_0 \cos\theta_0 - \omega_n t)\right], \tag{1}$$

where k_n - is the wave number, $n = 1,2$ according to the waves with frequencies ω_1 and ω_2, and r_0 is the radius-vector of the polar coordinate system.
Consider an incident plane wave in the spheroidal coordinate system [Skudrzyk, 1971]:

$$\exp\left[i(\omega_n t - k_n r_0 \cos\theta_0)\right] = -2\exp(i\omega_n t)\sum_{m=0}^{\infty}\sum_{l\ge m}^{\infty} i^{-l}\,\overline{S_{ml}}(k_n h_0, \eta_0)\overline{S_{ml}}(k_n h_0, \eta) R_{ml}^{(1)}(k_n h_0, \xi)\cos m(\varphi - \varphi_0),$$

where $\overline{S_{ml}}(k_n h_0, \eta)$ is the normalized angular first-order function and $R_{ml}^{(1)}(k_n h_0, \xi)$ is the radial spheroidal first-order function.
After the plane wave scattering on the spheroid, the scattered spheroidal wave of pressure will propagate as an outgoing wave [Kleshchyov & Klyukin, 1987]

$$p_{ns}(\xi, \eta, \varphi) = 2\exp(i\omega_n t)\sum_{m=0}^{\infty}\sum_{l\ge m}^{\infty} A_{ml}(k_n h_0, \xi_0)\overline{S_{ml}}(k_n h_0, \eta) R_{ml}^{(3)}(k_n h_0, \xi)\cos m\varphi, \tag{2}$$

where the coefficient $A_{ml}(k_n h_0, \xi_0)$ is dependent on boundary conditions on the spheroid surface, and $R_{ml}^{(3)}(k_n h_0, \xi)$ is the radial spheroidal third-order function.
In this case the spheroid is considered to be acoustically rigid, so the Neumann boundary condition must be applied on the surface:

$$\left(\frac{\partial p_{ni}}{\partial n} + \frac{\partial p_{ns}}{\partial n} \right)\Bigg|_{\xi=\xi_0} = 0 , \tag{3}$$

and the coefficient $A_{ml}(k_n h_0, \xi_0)$ will be determined by the following expression:

$$A_{ml}(k_n h_0, \xi_0) = -i^l \varepsilon_m \overline{S_{ml}}(k_n h_0, \eta_0) \frac{R_{ml}^{(1)'}(k_n h_0, \xi_0)}{R_{ml}^{(3)'}(k_n h_0, \xi_0)}$$

where $R_{ml}^{(1)'}(k_n h_0, \xi_0)$ and $R_{ml}^{(3)'}(k_n h_0, \xi_0)$ are the derivatives of the first- and third-order functions, $\varepsilon_m = 1$, for $m = 0$, $\varepsilon_m = 2$, for $m > 0$.
With the appearance of the scattered spheroidal wave, the total acoustic pressure of the primary field around the spheroid will have the form:

$$p^{(1)} = p_{ni} + p_{ns} = \left[\sum_{m=0}^{\infty} \sum_{l \geq m}^{\infty} B_{ml}(k_n h_0) \exp[i(\omega_n t - l\pi/2)] + \sum_{m=0}^{\infty} \sum_{l \geq m}^{\infty} D_{ml}(k_n h_0) \exp[i(\omega_n t - m\varphi)] \right] +$$

$$+ \left[\sum_{m=0}^{\infty} \sum_{l \geq m}^{\infty} B_{ml}(k_n h_0) \exp[-i(\omega_n t - l\pi/2)] + \sum_{m=0}^{\infty} \sum_{l \geq m}^{\infty} D_{ml}(k_n h_0) \exp[-i(\omega_n t - m\varphi)] \right] \tag{4}$$

where
$B_{ml}(k_n h_0) = 2\overline{S_{ml}}(k_n h_0, \eta_0)\overline{S_{ml}}(k_n h_0, \eta) R_{ml}^{(1)}(k_n h_0, \xi) \cos m(\varphi - \varphi_0)$,
$D_{ml}(k_n h_0) = 2A_{ml}(k_n h_0, \xi_0)\overline{S_{ml}}(k_n h_0, \eta_0) R_{ml}^{(3)}(k_n h_0, \xi) \cos m\varphi$.
To solve the problem of the non-linear interaction of the primary high-frequency waves, we combine expression (4) with its complex-conjugate part.
Nonlinear wave processes between incident and scattered waves surrounding the spheroid can be described with the inhomogeneous wave equation [Novikov et al., 1987]:

$$\nabla^2 p^{(2)} - \frac{1}{c_0^2} \frac{\partial^2 p^{(2)}}{\partial t^2} = -Q = -\frac{\varepsilon}{c_0^4 \rho_0} \frac{\partial^2 p^{(1)^2}}{\partial t^2} , \tag{5}$$

where Q is the volume density of the sources of secondary waves, c_0 is the sound velocity in the medium, ε is the quadratic nonlinearity parameter, ρ_0 is the density of the unperturbed medium, and $p^{(1)}$ and $p^{(2)}$ are the total acoustic pressures of the primary and secondary fields.
It is important to note that the waves of the primary field are the high frequency waves: incident plane waves p_i and scattered spheroidal waves p_s with angular frequencies ω_1 and ω_2. The waves of the secondary field are the waves that appear as a result of the non-linear interaction of initial high frequency waves. This includes the difference frequency

wave $\omega_2 - \omega_1 = \Omega$, the summation frequency wave $\omega_2 + \omega_1$, and the second harmonic waves $2\omega_1$, $2\omega_2$.

The wave equation (5) is solved by the method of successive approximations. In the first approximation, the solution is represented by the expression (4) for the total acoustic pressure of the primary field $p^{(1)}$. To determine solution in the second approximation $p^{(2)}$, the right-hand side of equation (5) should feature four frequency components: second harmonics of the incident waves ($2\omega_1$, $2\omega_2$) and ($\omega_1 + \omega_2$, $\omega_2 - \omega_1 = \Omega$).

The expression for the volume density of secondary waves sources at the difference frequency Ω is:

$$Q_- = \frac{2\Omega^2\varepsilon}{c_0^4\rho_0}\left[\sum_{m=0}^{\infty}\sum_{l\geq m}^{\infty} B_{ml}(k_1h_0)B_{ml}(k_2h_0)\cos\Omega t + \sum_{m=0}^{\infty}\sum_{l\geq m}^{\infty} B_{ml}(k_1h_0)D_{ml}(k_2h_0)\cos(\Omega t + l\pi/2 - m\varphi) + \right.$$

$$\left. + \sum_{m=0}^{\infty}\sum_{l\geq m}^{\infty} B_{ml}(k_2h_0)D_{ml}(k_1h_0)\cos(\Omega t + m\varphi - l\pi/2) + \sum_{m=0}^{\infty}\sum_{l\geq m}^{\infty} D_{ml}(k_1h_0)D_{ml}(k_2h_0)\cos\Omega t\right]. \quad (6)$$

To solve the inhomogeneous wave equation (5) with the right-hand side given by equation (6) in the second approximation, we seek the solution in the complex form

$$p_-^{(2)} = \frac{1}{2}P_-^{(2)}\exp(i(\Omega t + \delta) + (c.c.)). \quad (7)$$

Substitution of the expression (7) into the inhomogeneous wave equation (5) gives the inhomogeneous Helmholtz equation:

$$\nabla^2 P_-^{(2)} + k_-^2 P_-^{(2)} = -q_-(\xi,\eta,\varphi), \quad (8)$$

where k_- is the wave number of the difference frequency Ω, and

$$q_-(\xi,\eta,\varphi) = \frac{2\Omega^2\varepsilon}{c_0^4\rho_0}\left[\sum_{m=0}^{\infty}\sum_{l\geq m}^{\infty} B_{ml}(k_1h_0)B_{ml}(k_2h_0)\exp(i\Omega t) + \right.$$

$$+ \sum_{m=0}^{\infty}\sum_{l\geq m}^{\infty} B_{ml}(k_1h_0)D_{ml}(k_2h_0)\exp\left[i(\Omega t + l\pi/2 - m\varphi)\right] +$$

$$+ \sum_{m=0}^{\infty}\sum_{l\geq m}^{\infty} B_{ml}(k_2h_0)D_{ml}(k_1h_0)\exp\left[i(\Omega t + m\varphi - l\pi/2)\right] +$$

$$\left. + \sum_{m=0}^{\infty}\sum_{l\geq m}^{\infty} D_{ml}(k_1h_0)D_{ml}(k_2h_0)\exp(i\Omega t)\right].$$

The solution to the inhomogeneous Helmholts equation (8) has the form of a volume integral of the product of the Green function with the density of the secondary wave sources [Novikov et al., 1987] [Lyamshev & Sakov, 1992]:

$$P_{-}^{(2)}(\xi,\eta,\varphi)=\int_{V} q_{-}(\xi',\eta',\varphi')G(r_1)h_{\xi'}h_{\eta'}h_{\varphi'}d\xi' d\eta' d\varphi' \,, \tag{9}$$

where $G(r_1)$ is the Green function, r_1 is the distance between the current point of the volume $M'(\xi',\eta',\varphi')$ and the observation point $M(\xi,\eta,\varphi)$ (Fig.4), and $h_{\xi'}$, $h_{\eta'}$, $h_{\varphi'}$ are the scale factors [Corn & Corn, 1968]:

$$h_{\xi'}=h_0\sqrt{\frac{\xi'^2-\eta'^2}{\xi'^2-1}}\,,\ h_{\eta'}=h_0\sqrt{\frac{\xi'^2-\eta'^2}{1-\eta'^2}}\,,\ h_{\varphi'}=h_0\sqrt{(\xi'^2-1)(1-\eta'^2)}\,.$$

In the far field $r' << r$, the Green function is determined by the asymptotic expression

$$G(r_1)=\exp(-ik_{-}r_1)/r_1\approx\exp\left[-ik_{-}\left(h_0\xi-h_0\xi'\eta\eta'-h_0\xi'\sqrt{(1-\eta^2)(1-\eta'^2)}\right)\right]\Big/h_0\xi\,.$$

The integration in equation (9) is performed over the volume V occupied by the second wave sources and bounded in the spheroidal coordinates by the relations

$$\xi_0\le\xi'\le\xi_S\,,\qquad -1\le\eta'\le 1\,,\qquad 0\le\varphi'\le 2\pi\,.$$

This volume has the form of a spheroidal layer of the medium, stretching from the spheroid's surface to the non-linear interaction boundary (Fig.4). An external spheroid with coordinate ξ_S appears to be the boundary of this area. Coordinate ξ_S is defined by the size of the non-linear interaction area between the initial high-frequency waves. This size is inversely proportional to the coefficient of viscous sound attention associated with the corresponding pumping frequency. Beyond this area, the initial waves are assumed to attenuate linearly.

After the integration with respect to coordinates φ' and η' (considering the high-frequency approximation), equation (9) takes the form

$$P_{-}^{(2)}(\xi,\eta,\varphi)=P_{-1}^{(2)}(\xi,\eta,\varphi)+P_{-2}^{(2)}(\xi,\eta,\varphi)+P_{-3}^{(2)}(\xi,\eta,\varphi)+P_{-4}^{(2)}(\xi,\eta,\varphi)=$$

$$=C_{-}\frac{1}{k_{-}h_0\eta}\left[\int_{\xi_0}^{\xi_S}T\xi'\sin(k_{-}h_0\xi'\eta)d\xi'-\int_{\xi_0}^{\xi_S}T\frac{\sin(k_{-}h_0\xi'\eta)}{\xi'}d\xi'\right], \tag{10}$$

where

$$C_{-}=\frac{8h_0^2\pi\Omega^2\varepsilon\exp(-ik_{-}h_0\xi)}{c_0^4\rho_0\xi}\,,$$

$$T=\left[\sum_{m=0}^{\infty}\sum_{l\ge m}^{\infty}B_{ml}(k_1h_0)B_{ml}(k_2h_0)+\sum_{m=0}^{\infty}\sum_{l\ge m}^{\infty}B_{ml}(k_1h_0)D_{ml}(k_2h_0)\exp\left[i(l\pi/2-m\varphi)\right]+\right.$$

$$\left.+\sum_{m=0}^{\infty}\sum_{l\ge m}^{\infty}B_{ml}(k_2h_0)D_{ml}(k_1h_0)\exp\left[i(m\varphi-l\pi/2)\right]+\sum_{m=0}^{\infty}\sum_{l\ge m}^{\infty}D_{ml}(k_1h_0)D_{ml}(k_2h_0)\right]$$

(from here on, the time factor $\exp(i\Omega t)$ is omitted).

The expression (10) for the total acoustic pressure of the difference-frequency wave $P_{-}^{(2)}(\xi,\eta,\varphi)$ consists of four spatial components. The first component $P_{-1}^{(2)}(\xi,\eta,\varphi)$ corresponds to the part of the acoustic pressure of the difference-frequency wave, that is formed in the spheroidal layer of the non-linear interaction area by the incident high-frequency plane waves ω_1 and ω_2. The second component $P_{-2}^{(2)}(\xi,\eta,\varphi)$ describes the interaction of the incident plane wave of frequency ω_1 with the scattered spheroidal wave of frequency ω_2. The third component $P_{-3}^{(2)}(\xi,\eta,\varphi)$ corresponds to the interaction of the scattered plane wave of frequency ω_2 with the scattered spheroidal wave of ω_1. The fourth component $P_{-4}^{(2)}(\xi,\eta,\varphi)$ characterises the interaction of two scattered spheroidal waves with frequencies ω_1 and ω_2.

4. Results

To obtain the final expression of the total acoustic pressure of the difference-frequency wave $P_{-}^{(2)}(\xi,\eta,\varphi)$, consider the first spatial component $P_{-1}^{(2)}(\xi,\eta,\varphi)$ from equation (10), which characterises the non-linear interaction between incident plane waves of highfrequency:

$$P_{-1}^{(2)}(\xi,\eta,\varphi)=\frac{C_{-}}{k_{-}h_0\eta}\left[\int_{\xi_0}^{\xi_S}\sum_{m=0}^{\infty}\sum_{l\geq m}^{\infty}B_{ml}(k_1h_0)B_{ml}(k_2h_0)\xi^{'}\sin(k_{-}h_0\xi^{'}\eta)d\xi^{'}-\right.$$

$$\left.-\int_{\xi_0}^{\xi_S}\sum_{m=0}^{\infty}\sum_{l\geq m}^{\infty}B_{ml}(k_1h_0)B_{ml}(k_2h_0)\frac{\sin(k_{-}h_0\xi^{'}\eta)}{\xi^{'}}d\xi^{'}\right]. \quad (11)$$

It should be noted that this is the only component that gives no information about the scatterer. The boundaries of the integration layer are directly defined by the elongated spheroid shape.

Using representation of the plane wave in the spheroidal coordinate system and substituting $B_{ml}(k_nh_0)$, the expression (11) takes the form

$$P_{-1}^{(2)}(\xi,\eta,\varphi)=\frac{C_{-}}{k_{-}h_0\eta}\left[\int_{\xi_0}^{\xi_S}\exp\left[-ik_{-}h_0\xi^{'}\eta\right]\xi^{'}\sin(k_{-}h_0\xi^{'}\eta)d\xi^{'}-\int_{\xi_0}^{\xi_S}\exp\left[-ik_{-}h_0\xi^{'}\eta\right]\frac{\sin(k_{-}h_0\xi^{'}\eta)}{\xi^{'}}d\xi^{'}\right]. \quad (12)$$

After the final integration with respect to the coordinate $\xi^{'}$, the expression for the first component (12) has the form

$$P_{-1}^{(2)}(\xi,\eta,\varphi)=P_{-11}^{(2)}+P_{-12}^{(2)}+P_{-13}^{(2)}+P_{-14}^{(2)}, \quad (13)$$

where

$$P_{-11,-12}^{(2)}\approx\mp\frac{C_{-}}{2k_{-}^2h_0^2\eta(\eta_0\mp\eta)}\left[\xi_S\exp\left[ik_{-}h_0(\eta_0\mp\eta)\xi_S\right]-\xi_0\exp\left[ik_{-}h_0(\eta_0\mp\eta)\xi_0\right]\right],$$

$$P_{-13,-14}^{(2)}\approx\mp\frac{C_{-}}{2i}\left[-\mathrm{Ei}\left[-ik_{-}h_0(\eta_0\mp\eta)\xi_S\right]+\mathrm{Ei}\left[-ik_{-}h_0(\eta_0\mp\eta)\xi_0\right]\right],$$

and $\mathrm{Ei}(ax)=\int\frac{\exp(ax)}{x}dx$ is the integral exponential function.

From the expression (13) for the first component $P_{-1}^{(2)}(\xi,\eta,\varphi)$ of the total acoustic pressure of the difference-frequency wave, it follows that the scattering diagram of this component is determined by the function $1/(\eta_0 \pm \eta)$. This function depends on the coordinate η_0 or, the polar coordinate system, equivalent to the angle of incidence θ_0 of the highfrequency plane waves. The scattering diagram of the first component $P_{-1}^{(2)}(\xi,\eta,\varphi)$ are shown in Fig.5 for angle of incidence of the high-frequency plane waves $\theta_0 = 30^0$ $(k\_h_0 = 5)$.

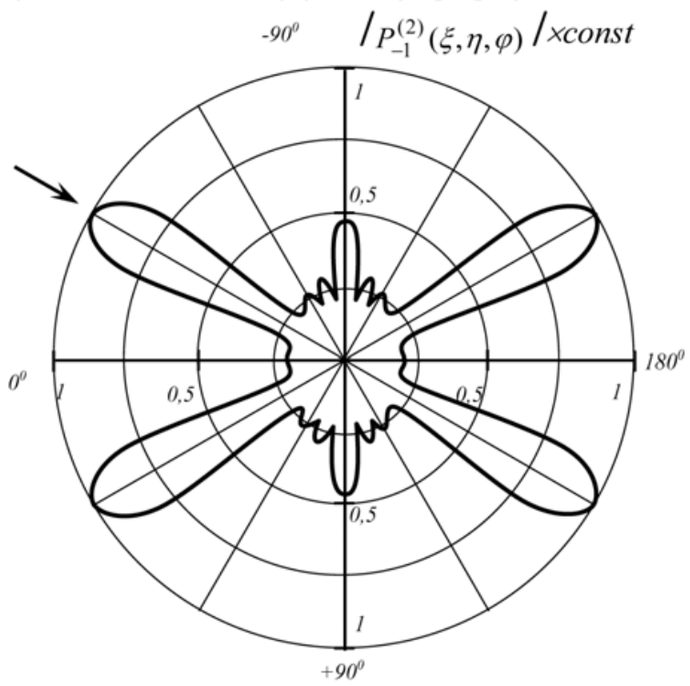

Fig. 5. Scattering diagram of the spatial component $P_{-1}^{(2)}(\xi,\eta,\varphi)$ of the total acoustic pressure produced by the difference-frequency wave by a rigid elongated spheroid for: f_2 =1000 kHz, f_1 =880 kHz, $F\_$ =120 kHz, k_h_0 =5, $\theta_0 = 30^0$, $k_{1,2}h_0 \approx 40, h_0$ =0,01 м, ξ_0 =1,005 (relations axis - 1:10), ξ =7.

In the direction of the angle of incidence (with respect to the *z*-axis), the scattering diagrams have major maximums. Increase of the amplitude of the spheroidal wave produced by the scatterer leads to additional maximums in lateral directions (irrespective of the angle of incidence). This result is connected with the increase of the function $1/\eta$. Increasing the extent of the interaction region (the coordinate ξ_S) results in the narrowing of the scattering lobes; this scenario corresponds to increasing the size of the re-radiating volume around the scatterer.

The elongated spheroid has radial dimension $\xi_0 = 1{,}005$ with the semi-axes correlation 1:10. Acoustic pressure of the difference frequency wave has been calculated in the far field of the scattering spheroid, i.e. in the Fraunhofer region.

Therefore, the scattering field can be considered as being shaped by. Shadowing of the secondary waves sources by the scatterer itself can occur in the Rayleigh region. Here it is necessary to take into account wave dimensions of the scatterer as well as the distance to the point of observation $M(\xi,\eta,\varphi)$. In the cases presented in this contribution, the point of

observation was at radial distances $\xi = 7$ and 15, which exceeded the length of the elongated spheroid by an order magnitude.

Now consider the second $P_{-2}^{(2)}(\xi,\eta,\varphi)$ and third $P_{-3}^{(2)}(\xi,\eta,\varphi)$ components from the equation (10) for the total acoustic pressure of the difference-frequency wave, these components characterise the non-linear interaction of the incident plane waves with the scattered spheroidal ones waves:

$$P_{-2}^{(2)}(\xi,\eta,\varphi) = \frac{C_-}{k_- h_0 \eta}\left[\int_{\xi_0}^{\xi_S}\sum_{m=0}^{\infty}\sum_{l\geq m}^{\infty} B_{ml}(k_1h_0)D_{ml}(k_2h_0)\exp\left[i(l\pi/2-m\varphi)\right]\xi^{'}\sin(k_-h_0\xi^{'}\eta)d\xi^{'} - \right.$$

$$\left. - \int_{\xi_0}^{\xi_S}\sum_{m=0}^{\infty}\sum_{l\geq m}^{\infty} B_{ml}(k_1h_0)D_{ml}(k_2h_0)\exp\left[i(l\pi/2-m\varphi)\right]\frac{\sin(k_-h_0\xi^{'}\eta)}{\xi^{'}}d\xi^{'}\right]. \qquad (14)$$

Values of $B_{ml}(k_nh_0)$ and $D_{ml}(k_nh_0)$ are substituted into equation (14) and the plane wave expansion is used. For the axially symmetrical scattering problem (perfect spheroid), the high-frequency asymptotic forms the angular spheroidal 1st- order function $S_{ml}(k_nh_0,\eta)$ and the radial spheroidal 3rd - order function $R_{ml}^{(3)}(k_nh_0,\xi^{'})$ [Kleshchyov & Klyukin, 1987], [Abramovitz & Stegun, 1971]:

$$R_{ml}^{(3)}(k_nh_0,\xi^{'}) \underset{k_nh_0\xi^{'}\to\infty}{\approx} \frac{i^{-l-1}}{k_nh_0\xi^{'}}\exp\left[ik_nh_0\xi^{'}\right].$$

Then equation (11) takes the form

$$P_{-2}^{(2)}(\xi,\eta,\varphi) \approx \frac{2iC_-A(k_2h_0)}{k_-k_2h_0^2\eta\sqrt{2(1-\eta)}}\left[\int_{\xi_0}^{\xi_S}\exp\left[-i(k_2h_0-k_1h_0\eta_0)\xi^{'}\right]\sin(k_-h_0\xi^{'}\eta)d\xi^{'} - \right.$$

$$\left. - \int_{\xi_0}^{\xi_S}\exp\left[-i(k_2h_0-k_1h_0\eta_0)\xi^{'}\right]\frac{\sin(k_-h_0\xi^{'}\eta)}{\xi^{'2}}d\xi^{'}\right]. \qquad (15)$$

After the final integration [Prudnikov et al., 1983], the expression for the 2nd component of the total acoustic pressure of the difference-frequency wave takes the form

$$P_{-2}^{(2)}(\xi,\eta,\varphi) = P_{-21}^{(2)} + P_{-22}^{(2)} + P_{-23}^{(2)} + P_{-24}^{(2)}, \qquad (16)$$

where

$$P_{-21,-22}^{(2)} \approx \mp\frac{iC_-A(k_2h_0)}{2k_-k_2h_0^2\eta\sqrt{(1-\eta_0)(1-\eta)}}\left[\frac{\exp(iu_2\xi_S)-\exp(iu_2\xi_0)}{u_2}\right],$$

$$P_{-23,-24}^{(2)} \approx \mp\frac{C_-A(k_2h_0)}{2k_-k_2h_0^2\eta\sqrt{(1-\eta_0)(1-\eta)}}\left[\frac{\exp(-iu_2\xi_S)}{\xi_S} - \frac{\exp(iu_2\xi_0)}{\xi_0} - u_2\left[\mathrm{Ei}(-iu_2\xi_S)-\mathrm{Ei}(-iu_2\xi_0)\right]\right],$$

$$u_2 = (k_2h_0 - k_1h_0\eta_0 \mp k_-h_0\eta).$$

The expression for the 3rd component $P_{-3}^{(2)}(\xi,\eta,\varphi)$ is similar to the expression (15). An analysis of equation (15) shows that the behaviour of scattering diagrams for the components $P_{-2}^{(2)}(\xi,\eta,\varphi)$ and $P_{-3}^{(2)}(\xi,\eta,\varphi)$ is determined mainly by the function $1/\eta\sqrt{(1-\eta_0)(1-\eta)}$, where the dependence on the angle of incident θ_0 (that is η_0) is not clear. The scattering diagram of these components are shown in Fig.6, for $\theta_0 = 30^0$ $(k\_h_0 = 5)$. These diagrams have maximums in the backward and side directions (0^0 and $\pm 90^0$). The increase of the wave size of the spheroidal scatterer leads to additional maximums, which depend on the angle of incident of the high-frequency plane waves.

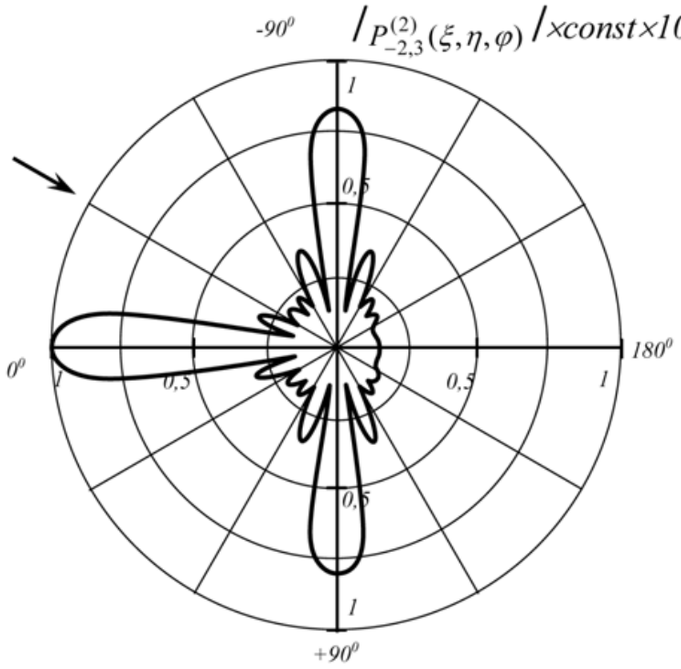

Fig. 6. Scattering diagram of the spatial components $P_{-2}^{(2)}(\xi,\eta,\varphi)$, $P_{-3}^{(2)}(\xi,\eta,\varphi)$ by a rigid elongated spheroid for: f_2 = 1000 kHz, f_1 =880 kHz, $F\_$ =120 kHz, k_h_0 =5, $\theta_0 = 30^0$, ξ_0 =1.005, ξ =7.

Now, we consider the fourth component $P_{-4}^{(2)}(\xi,\eta,\varphi)$ of the total acoustic pressure of the difference-frequency wave. This component characterises the non-linear interaction of the scattered spheroidal waves with frequencies ω_1 and ω_2:

$$P_{-4}^{(2)}(\xi,\eta,\varphi) = \frac{C\_}{k\_h_0\eta}\left[\int_{\xi_0}^{\xi_S}\sum_{m=0}^{\infty}\sum_{l\geq m}^{\infty} D_{ml}(k_1h_0)D_{ml}(k_2h_0)\xi' \sin(k\_h_0\xi'\eta)d\xi' - \right.$$

$$\left. - \int_{\xi_0}^{\xi_S}\sum_{m=0}^{\infty}\sum_{l\geq m}^{\infty} D_{ml}(k_1h_0)D_{ml}(k_2h_0)\frac{\sin(k\_h_0\xi'\eta)}{\xi'}d\xi'\right]. \qquad (17)$$

After some algebraic manipulations, equation (17) takes the form

$$P_{-4}^{(2)}(\xi,\eta,\varphi) = P_{-41}^{(2)} + P_{-42}^{(2)} + P_{-43}^{(2)} + P_{-44}^{(2)}, \tag{18}$$

where

$$P_{-41,-42}^{(2)} \approx \mp \frac{C_{-}A(k_2h_0)A(k_2h_0)}{2ik_{-}k_2k_1h_0^2\eta(1-\eta_0)(1-\eta)}\left[-u_4\left[\mathrm{Ei}(-iu_4\xi_S)-\mathrm{Ei}(-iu_4\xi_0)\right]\right],$$

$$P_{-43,-44}^{(2)} \approx \mp \frac{C_{-}A(k_2h_0)A(k_2h_0)}{4ik_{-}k_2k_1h_0^2\eta(1-\eta_0)(1-\eta)}\left[iu_4\left(\frac{\exp(-iu_4\xi_S)}{\xi_S}-\frac{\exp(iu_4\xi_0)}{\xi_0}\right)+u_4^2\left[\mathrm{Ei}(-iu_4\xi_S)-\mathrm{Ei}(-iu_4\xi_0)\right]\right],$$

$u_4 = (k_{-}h_0 \mp k_{-}h_0\eta)$.

The scattering diagram of the fourth component $P_{-4}^{(2)}(\xi,\eta,\varphi)$ are shown in Fig.7, for $\theta_0 = 30^0$ $(k_{-}h_0 = 5)$. Their configuration is primarily determined by the function $1/\eta(1-\eta_0)(1-\eta)$ of equation (18). As indicated above, this function has a maximum in the backward direction and slightly depends on the angle of incidence. Increasing of the spheroidal scatterer wave size results increases lateral scattering.

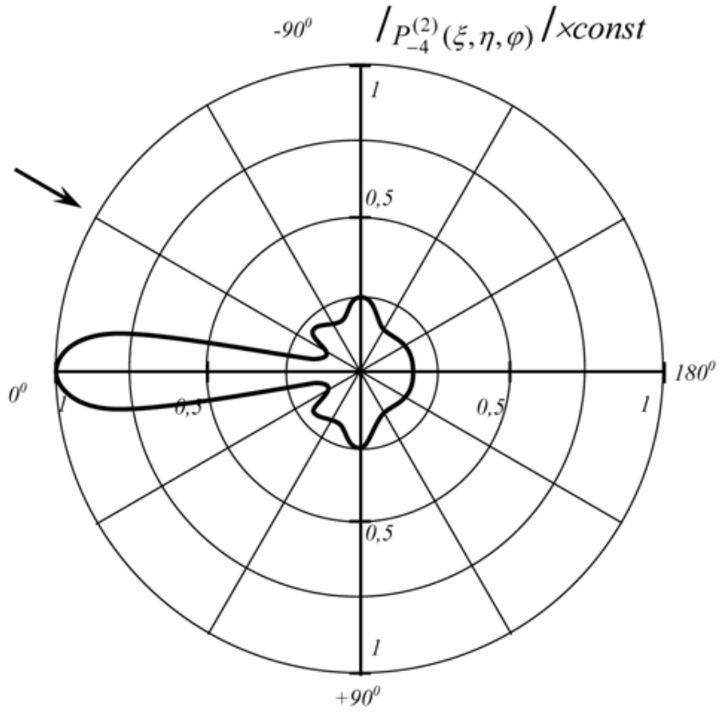

Fig. 7. Scattering diagram of the spatial component $P_{-4}^{(2)}(\xi,\eta,\varphi)$ by a rigid elongated spheroid for: f_2 = 1000 kHz, f_1 =880 kHz, F_{-} =120 kHz, $k_{-}h_0$ =5, $\theta_0 = 30^0$, ξ_0 =1.005, ξ =7.

Fig.8 presents the scattering diagram of the total acoustic pressure in the difference-frequency wave $P_{-}^{(2)}(\xi,\eta,\varphi)$ according to the asymptotic expressions for spatial components. In this case, the angle of incidence is $\theta_0 = 30^0$ $(k_{-}h_0 = 5)$, and the coordinate $\xi = 7$.

Fig.9 shows wave scattering diagrams of difference frequency $P_{-}^{(2)}(\xi,\eta,\varphi)$ on rigid elongated spheroid ξ_0 =1,005 with different incidence angle values of inflation incident waves $\theta_0 = 0^0$; 90^0.

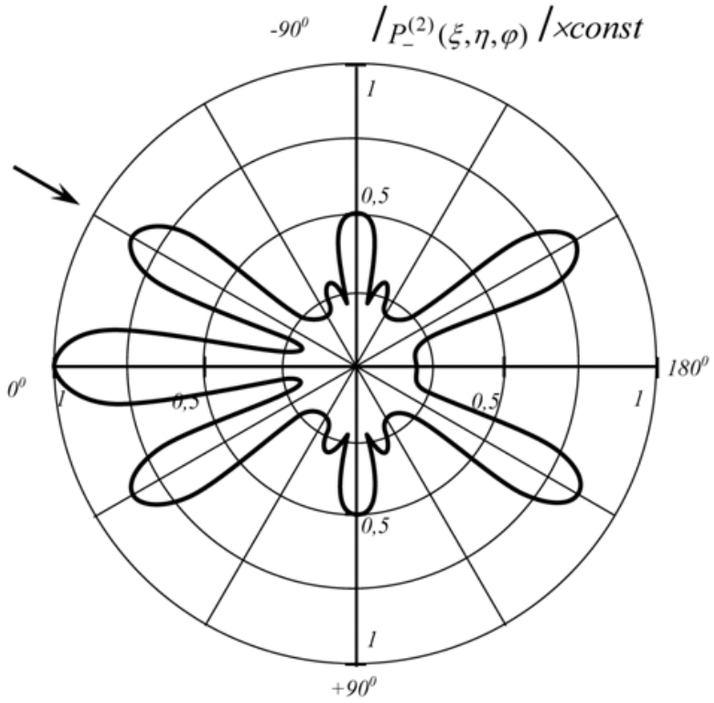

Fig. 8. Scattering diagram of the total acoustic pressure the difference-frequency wave $P_{-}^{(2)}(\xi,\eta,\varphi)$ by a rigid elongated spheroid for: f_2 = 1000 kHz, f_1 =880 kHz, F_{-} =120 kHz, $k_{-}h_0$ =5, $\theta_0 = 30^0$, ξ_0 =1,005, ξ =7.

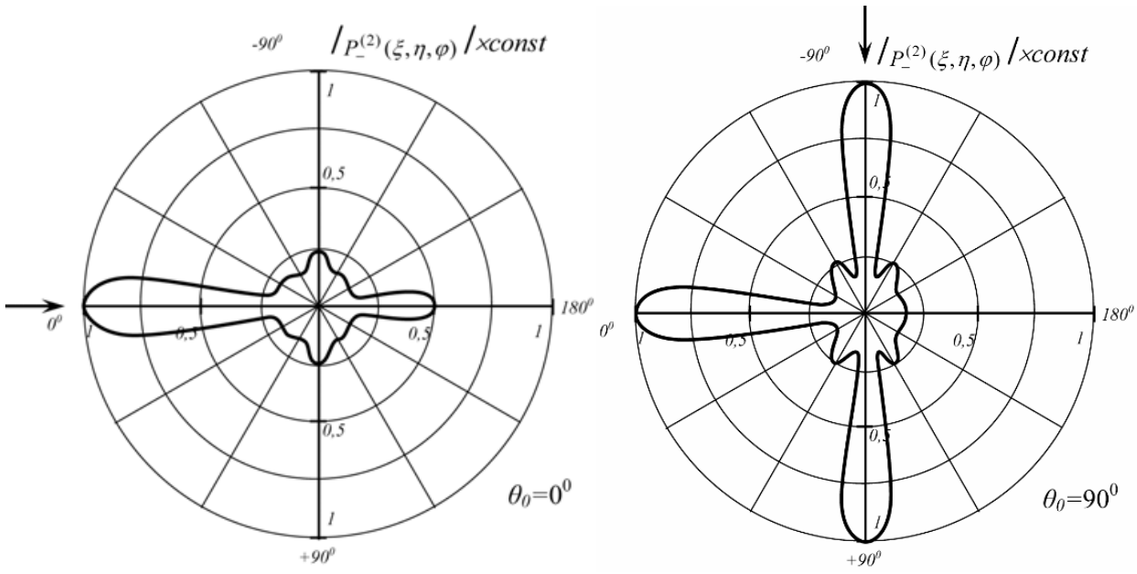

Fig. 9. Scattering diagrams of the total acoustic pressure the difference-frequency wave $P_{-}^{(2)}(\xi,\eta,\varphi)$ by a rigid elongated spheroid for: f_2 = 1000 kHz, f_1 =880 kHz, F_{-} =120 kHz, $k_{-}h_0$ =5, ξ_0 =1,005, ξ =7, $\theta_0 = 0^0$; 90^0.

With incidence angle $\theta_0 = 0^0$ diagrams have got the basic maximums back, with the increase of spheroid wave dimension, the modest lateral scattering appears. With incidence angle $\theta_0 = 60^0$ diagrams are of the similar form $\theta_0 = 30^0$, with conformable maximums in decrease direction, in mirrorlike, as well as back.

With incidence angle $\theta_0 = 90^0$ diagrams have got the basic maximums back and lateral directions. With the wave dimension growth, modest intermediate levels can be observed. It follows from Fig.9 that angle value change θ_0 leads generally to the change of maximums position in the line of incidence and reflex angle.

It is emphasized that the figures illustrate the dependence of acoustic pressure $P_{-}^{(2)}(\xi,\eta,\varphi)$ on the polar angle $\theta = \arccos\eta$ but not on the angle of asymptote of the hyperbola η. This presentation is conventionally employed for the scattering diagrams in spheroidal coordinates [Cpence & Ganger, 1951], [Kleshchyov & Sheiba, 1970].

The diagrams are presented in the *xoz* plane (Fig.4). Polar angle θ varies in the range 0^0 to 360^0; the value of the angle $\theta = 0^0$ corresponds to the position of x axis, and the value $\theta = 90^0$ corresponds to *z* axis. The arrow here shows the direction of the initial plane wave incidence. The axisymmetry of the diagrams with respect to x axis has been taken into account and two diagrams with positive and negative directions of the angle $\theta = \pm 180^0$ have been combined.

Fig.10 shows a spatial simulation of the scattering diagram of the total acoustic pressure $P_{-}^{(2)}(\xi,\eta,\varphi)$ for $\theta_0 = 30^0$ ($k\_h_0 = 5$, $\xi = 7$, an arrow indicates the direction of the initial wave incidence). It is a surface of revolution, and the rotation axis is the larger axis of the elongated spheroid, that is the *x*- axis.

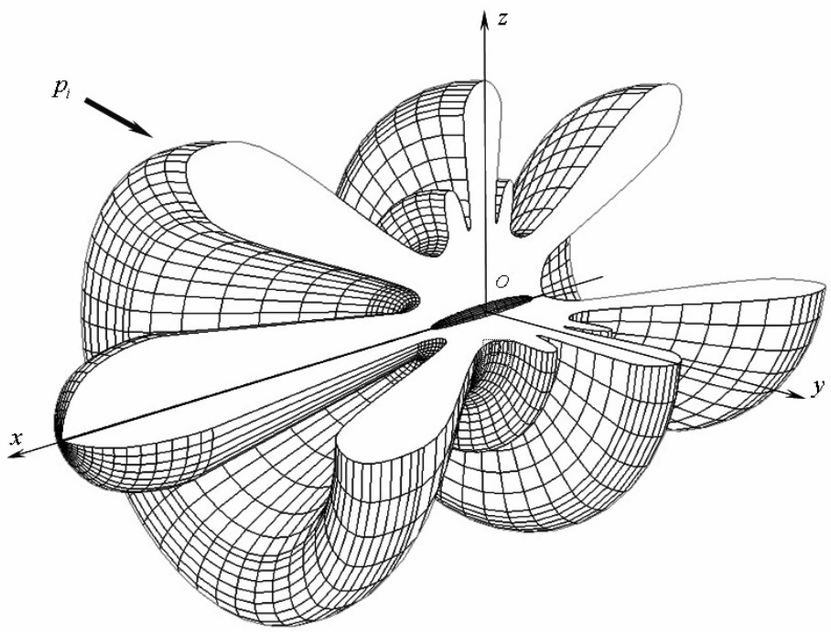

Fig. 10. Spatial model of scattering diagram of the total acoustic pressure the difference-frequency wave $P_{-}^{(2)}(\xi,\eta,\varphi)$ by a rigid elongated spheroid for: f_1 =880 kHz, F_{-} =120 kHz, k_h_0 =5, $\theta_0 = 30^0$, ξ =7.

5. Discussion

Although investigation of the linear scattering of acoustic waves by the elongated spheroid has been considered previously, results of the scattering of the nonlinearly interacting acoustic wave were not reported. In most previous publications, the problem is investigated when the angles of incidence of acoustic waves are $\theta = 0^0$ and 90^0 [Kleshchyov & Sheiba, 1970], [Tetyuchin & Fedoryuk, 1989].

In article [Kleshchyov & Sheiba, 1970] the calculated diagrams of plane acoustic wave scattering by a similar size spheroid ($\xi_0 = 1{,}005$, $kh_0 = 10$) at angle of incidence $\theta = 30^0$ are presented. Also in this work the scattering diagram has maximums symmetrical to the angle of incidence (mirror lobes) with respect to z axis [Burke, 1966], [Boiko, 1983]. At angle of incidence $\theta = 0^0$ forward scattering dominates. The basic maximum is aligned with 140^0. When the angle of incidence is $\theta = 90^0$ (lateral incidence), there are only two maximums – forward and backward.

An analysis of the acoustic pressure distribution of the difference-frequency wave scattered field shows that the scattering diagrams have maximums in a backward direction. In direction to the angle of incidence, in lateral and transverse directions, plane waves have maximums. Incident high-frequency plane waves form the scattering field in backward and forward directions, and scattered spheroidal waves form the scattering field in transverse direction. An increase in the wave size of the spheroidal scatterer changes maximum levels, and an increase in the size of the interacting area around the elongated spheroidal scatterer leads to narrowing of these maximums.

It is important to note that in this work we considered the case when the scattered field is generated by the secondary wave sources located in the volume around the spheroid. In the case of the linear scattering, these sources are located on the surface of the spheroid. The mirror maximums 30^0 and 150^0 appear as a result of the asymptotics of the first spatial sum $P_{-1}^{(2)}(\xi,\eta,\varphi)$ as confirmed in [2]. Therefore, the plotted scattering diagrams are in conformity with the results of 90^0 [Burke, 1966], [Kleshchyov & Sheiba, 1970], [Boiko, 1983], [Tetyuchin & Fedoryuk, 1989].

As for the numerical evaluation of the acoustic pressure, it is necessary to note the following. In view of the complexity of mathematical calculations, the obtained asymptotics allow for qualitative evaluation of the spatial distribution of the acoustic pressure in the scattered field. It would be more adequate to compare the results with experimental data. Unfortunately, experiments in non-linear conditions have not been carried out. For the sake of better understanding of contribution of the separated sums into the cumulative acoustic field, results were presented for two values of the wave dimension and the angle of incidence.

It should be noted, that description of wave processes in spheroidal coordinates have several peculiarities. For example, comparing the acoustic pressure distribution at the distance from the scatterer, the results given in [Abbasov & Zagrai, 1994], [Abbasov & Zagrai, 1998], [Abbasov, 2007] can be taken. Spheroidal coordinates in a far field transform into spherical ones $(h_0 \to 0)$ and $P_{-}^{(2)}(\xi,\eta,\varphi) \to P_{-}^{(2)}(r,\theta,\varphi)$. The results of this research are in agreement with results of prior studies of the scattering process described in spherical coordinates.

6. Conclusion

Summing up the secondary field studies on the difference frequency wave with interacting acoustic wave scattering on elongated spheroid, it should be noted that:

- the statement of the problem has been formulated and problem peculiarities of scattering in elongated spheroidal coordinates has been described, the solution of non-homogeneous wave equation in the second approximation and Helmholtz nonhomogeneous equation on the difference frequency wave has been obtained;
- high-frequency asymptotic expressions of general acoustic pressure of difference frequency wave have been obtained; they consist of spacing terms, characterizing nonlinear interaction between incident plane and scattered spheroidal waves;
- the assumption diagrams of difference frequency wave scattering on different distances from spheroidal scatterer, for different incident angles and different wave dimensions: $k\_h_0 = 0{,}5 \div 1$, incident angles $\theta_0 = 0^0$, 30^0, 60^0, 90^0, radial distances ξ =3; 7; 15, have been obtained;
- the obtained diagrams of difference frequency wave scattering have basic maximums in back, lateral directions and in the incidence and reflex line (reflection lobe) of inflation waves, three-dimensional diagram models of difference frequency wave scattering on elongated spheroid have been featured.

The method of successive approximations has been used for the description of wave processes with weak non-linearity. The diagrams are presented that illustrate the distribution of acoustic pressure of the scattered field. In view of the obtained theoretical results, the method of successive approximations is an adequate tool for solving the problem of the scattering of non-linearly interacting waves by an elongated spheroid.

7. References

Abbasov, I.B. (2007). *Scattering nonlinear interacting acoustic waves: sphere, cylinder and a spheroid*. Fizmatlit, Moscow, 160p.

Abbasov, I.B., Zagrai, N.P. (1994). Scattering of interacting plane waves by a sphere. *Acoust. Phys.* Vol. 40, No. 4, P. 473-479.

Abbasov, I.B., Zagrai, N.P. (1998). The investigation of the second field of the summarized frequency originated from scattering of nonlinearly interacting sound waves at a rigid sphere. *Journal of Sound and Vibration.* Vol. 216, No. 1, P. 194-197.

Abramovitz, M., Stegun, I. (1971). *Handbook of special functions with formulas, graphs, and mathematical tables*. Dover, New York, 830p.

Andebura, V. A. (1969). Acoustic properties of spheroidal radiators. *Akust. Zh.* Vol. 15, No.44, P. 513-522.

Andebura, V. A. (1976). About akustic - mechanical characteristics spheroidal a radiator and scatterer. *Akust. Zh.* Vol. 22, No. 4, P. 481-486.

Babailov, E.P., Kanevsky V.A. (1988). Sound scattering the gas-filled spheroidal bubble of fishes. *Akust. Zh.* Vol. 34, No. 1, P. 19-23.

Belkovich, V. M, Grigoriev, V. A, Katsnelson, B.G., Petnikov, V.G. (2002). About possibilities of use of acoustic diffraction in monitoring problems cetaceans. *Akust. Zh.* Vol. 48, No. 2, P. 162-166.

Boiko, A.I. (1983). The scattering of plane sound wave from thin revolve body. *Akust. Zh.* Vol. 29, No. 3, P. 321-325.

Burke, J.E. (1966). Long-wavelength scattering by hard spheroids. *Journ. Acoust. Soc. Amer*. Vol. 39, No. 5, P. 826-831.

Chertock, G. (1961). Sound radiation from circular pistons of elliptical profile. *Journ. Acoust. Soc. Amer.* Vol. 33, No. 7, P. 871-8876.

Corn, H., Corn, T. (1961). *Mathematical Handbook*. cMgraw-Hill Book Company, New York. 720p.

Cpence, R., Ganger, S. (1951). The scattering of sound from a prolate spheroid. *Journ. Acoust. Soc. Amer*. Vol. 23, No. 6, P. 701-706.

Fedoryuk, M.V. (1981). The scattering of sound wave from thin acoustically rigid revolve body. *Akust. Zh.* Vol. 27, No. 4, P. 605-609.

Guyer, R.A., Johnson, P.A. (1999). Nonlinear mesoscopic elasticity evidence for a new class of materials. *Physics Today*. Vol. 52, No. 4, P. 30-36.

Haslett, R. (1962). Determination of the acoustic scatter patterns and cross sections of fish models and ellipsoids. *Brit. Journ. Appl. Phys.* Vol. 13, No. 12, P. 611-620.

Kleshchyov, A.A, Sheiba, L.S. (1970). The scattering of sound wave from an ideal elongated spheroids. *Acoust. Phys.(Akust. Zh.)* Vol. 16, No.2, P. 264-268.

Kleshchyov, A.A. (1992). *Hydroacoustic scatterers*. Sudostroenie. St. Peterburg. 248p.

Kleshchyov, A.A. (2004). Physical model of sound scattering by jamb of fishes who is at border of section of. *Akust. Zh.* Vol. 50, No. 4, P. 512-515.

Kleshchyov, A.A., Clyukin, I.I. (1987). *The foundation of hydroacoustic*. Sudostroenie, Leningrad. 224p.

Kleshchyov, A.A., Rostovtsev, D.M. (1986). Sound scattering elastic and liquid ellipsoidal rotation shells. *Akust. Zh.* Vol. 32, No. 5, P. 691-694.

Kuzkin, V.M. (2003). Scattering of sound waves on a body in плоскослоистом a wave guide. *Akust. Zh.* Vol. 49, No. 1, P. 77-84.

Lebedev, A.V., Ostrovsky,i L.A., Sutin A.M. (2005). Nonlinear acoustic spectroscopy of local defects in geomaterials. *Akust. Zh.* Vol. 51, No. add., P. 103-117.

Lebedev, A.V., Salin, B.M. (1997). An experimental method of definition of dispersion section of the elongated bodies. *Akust. Zh.* Vol. 43, No. 3, P. 376-385.

Lyamshev, L.M., Sakov, P.V. (1992). Nonlinear scattering of sound from an pulsted sphere. *Soviet Physics Acoustics,* Vol. 38, No. 1, P. 51-57.

Novikov, B.K., Rudenko, O.V., Timoshenko, V.I. (1987). *Nonlinear underwater acoustic*. Acoustical Society of America, New York, 264 p.

Prudnikov, A.P., Brychkov, Yu. A., Marichhev, O.I. (1983). *Integrals and rows*. Nauka. Moscow. 752p.

Skudrzyk, E. (1971). *The foundations of acoustics*. Springer, New York, 542p.

Stanton, T.K. (1989). Simple approximate formulas for backscattering of sound by spherical and elongated objects. *Journ. Acoust. Soc. Amer*. Vol. 86, No. 4, P. 1499-1510.

Tetyuchin, M.Yu., Fedoryuk, M.V. (1989). The diffraction of plane sound wave from a elongated rigid revolved body in the liquid. *Akust. Zh.* Vol. 35, No. 1, P. 126-130.

Tikhonov, A.N., Samarskyi, A.A. (1966). *The equations of mathematical physics*. Nauka, Moscow. 724p.

Weksler, N.D., Dubious, B., Lave, A. (1999). The scattering of acoustic wave from an ellipsoidal shell. *Akust. Zh.* Vol. 45, No. 1, P. 53-58.

Werby, M.F., Green, L.H. (1987). Correspondence between acoustical scattering from spherical and end-on incidence spherical shells. *Journ. Acoust. Soc. Amer.* Vol. 81, No. 2, P. 783-787.

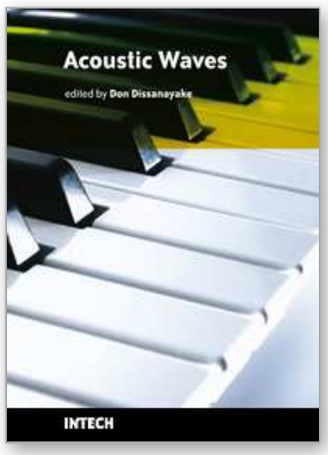

Acoustic Waves
Edited by Don Dissanayake

ISBN 978-953-307-111-4
Hard cover, 434 pages
Publisher Sciyo
Published online 28, September, 2010
Published in print edition September, 2010

SAW devices are widely used in multitude of device concepts mainly in MEMS and communication electronics. As such, SAW based micro sensors, actuators and communication electronic devices are well known applications of SAW technology. For example, SAW based passive micro sensors are capable of measuring physical properties such as temperature, pressure, variation in chemical properties, and SAW based communication devices perform a range of signal processing functions, such as delay lines, filters, resonators, pulse compressors, and convolvers. In recent decades, SAW based low-powered actuators and microfluidic devices have significantly added a new dimension to SAW technology. This book consists of 20 exciting chapters composed by researchers and engineers active in the field of SAW technology, biomedical and other related engineering disciplines. The topics range from basic SAW theory, materials and phenomena to advanced applications such as sensors actuators, and communication systems. As such, in addition to theoretical analysis and numerical modelling such as Finite Element Modelling (FEM) and Finite Difference Methods (FDM) of SAW devices, SAW based actuators and micro motors, and SAW based micro sensors are some of the exciting applications presented in this book. This collection of up-to-date information and research outcomes on SAW technology will be of great interest, not only to all those working in SAW based technology, but also to many more who stand to benefit from an insight into the rich opportunities that this technology has to offer, especially to develop advanced, low-powered biomedical implants and passive communication devices.

How to reference
In order to correctly reference this scholarly work, feel free to copy and paste the following:

Iftikhar Abbasov (2010). Research of the Scattering of Non-Linearly Interacting Plane Acoustic Waves by an Elongated Spheroid, Acoustic Waves, Don Dissanayake (Ed.), ISBN: 978-953-307-111-4, InTech, Available from: http://www.intechopen.com/books/acoustic-waves/research-of-the-scattering-of-non-linearly-interacting-plane-waves-by-an-elongated-spheroid

INTECH
open science | open minds

InTech Europe
University Campus STeP Ri
Slavka Krautzeka 83/A
51000 Rijeka, Croatia

InTech China
Unit 405, Office Block, Hotel Equatorial Shanghai
No.65, Yan An Road (West), Shanghai, 200040, China
中国上海市延安西路65号上海国际贵都大饭店办公楼405单元

Phone: +385 (51) 770 447
Fax: +385 (51) 686 166
www.intechopen.com

Phone: +86-21-62489820
Fax: +86-21-62489821

IntechOpen

IntechOpen